This manuscript has been published in the Journal of the Mechanical Behaviour of Biomedical Materials, 2015 Oct; 50:131-49. doi: 10.1016/j.jmbbm.2015.05.026. Epub 2015 Jun 16.

GRAPHICAL ABSTRACT

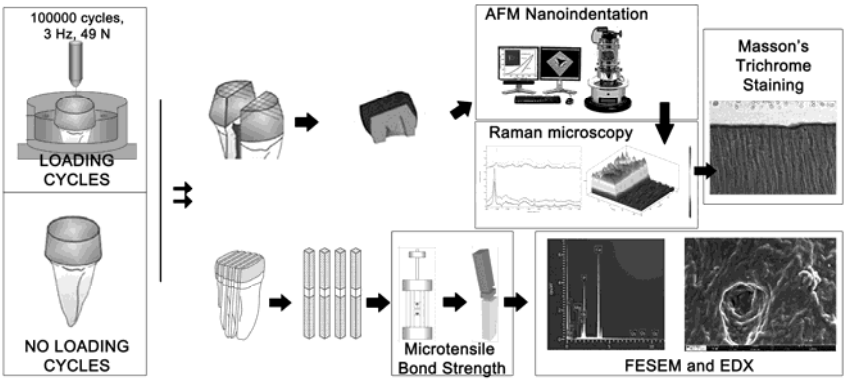

Title: Functional and molecular structural analysis of dentine interfaces promoted by a Zn-doped self-etching adhesive and an *in vitro* load cycling model.

Short title: Remineralisation of Zn-doped self-etching adhesives and load cycling.

Authors: Manuel Toledano[1*], Fátima S. Aguilera[1], Estrella Osorio[1], Inmaculada Cabello[1], Manuel Toledano-Osorio[1], Raquel Osorio[1].

Institution: [1]University of Granada, Faculty of Dentistry, Dental Materials Section.

Address: [1]University of Granada, Faculty of Dentistry, Dental Materials Section
Colegio Máximo de Cartuja s/n
18071 – Granada - Spain.

Corresponding author: Prof. Manuel Toledano
University of Granada, Faculty of Dentistry
Dental Materials Section
Colegio Máximo de Cartuja s/n
18071 – Granada - Spain.
Tel.: +34-958243788
Fax: +34-958240809
Email: toledano@ugr.es

ABSTRACT

The aim of this study was to evaluate if mechanical cycling influences bioactivity and bond strength at the resin-dentine interface after bonding with Zn-doped self-etching adhesives. Sound dentine surfaces were bonded with Clearfil SE Bond (Kuraray, Tokyo, Japan) (SEB), and 10 wt% ZnO microparticles (Panreac Química, Barcelona, Spain) or 2 wt% $ZnCl_2$ (Sigma Aldrich, St Louis, MO, USA) were added into the SEB primer (P) or bonding (Bd) for Zn-doping. Bonded interfaces were stored in simulated body fluid during 24 h, and then tested or submitted to mechanical loading. Microtensile bond strength (MTBS) was assessed for the different groups. Debonded dentine surfaces were studied by field emission scanning electron microscopy (FESEM). Remineralisation of the bonded interfaces was assessed nano-indentation, Raman spectroscopy/cluster analysis, and Masson's trichrome staining. Load cycling (LC) increased the percentage of adhesive failures in all groups. LC increased the Young's modulus (Ei) at the hybrid layer (HL) when SEB, SEB·P-ZnO and SEB·P-$ZnCl_2$ were applied, but decreased when both ZnO and $ZnCl_2$ were incorporated into the bonding (SEB·Bd). In general, Ei was higher and more uniform when Zn compounds were incorporated into the primer (SEB·P). ZnO promoted an increase, and $ZnCl_2$ a decrease, of both the relative presence of minerals and crystallinity, after LC. Mechanical loading increased collagen crosslinking at the interface with both SEB·P-ZnO and SEB·P-$ZnCl_2$. The ratios which reflect the nature of collagen increased, in general, at both HL and BHL after LC, confirming recovery, better organization, improved structural differences and collagen quality. After loading, trichrome staining reflected a deeper demineralised dentine fringe when Zn-doped compounds were incorporated into SEB·Bd. Multiple Zn-rich phosphate deposits and salt formations were detected.

Mineral precipitates nucleated in multilayered platforms or globular formations on peritubular and intertubular dentine.

Key words: remineralisation, dentine, load cycling, self-etch adhesives, strength.

1. INTRODUCTION.

Dentine is a mineralised connective tissue and consists of approx. 70% hydroxyapatite, 20% organic material and 10% water (by weight) (Cao et al., 2005). Accordingly, demineralisation of dentine is the process of removing minerals ions from the apatite latticework leaving the collagen fibers without support except for the water contained within the dentine (Bertassoni et al., 2011). Demineralisation of dentine, or dentine conditioning, is used as a surface preparation step to improve adhesion for a variety of procedures in restorative dentistry (Toledano et al., 2001). The primer assists the adhesive to flow into and penetrate the conditioned tooth surface, and often it contains a hydrophilic portion that interacts with the moisture present in the tooth structure, as well as a hydrophobic end that provides bonding sites for the methacrylate monomers in the bonding resin (Tay and Pashley, 2001). Dentine demineralisation and further resin infiltration are clinically required to promote resin-dentine bonding. The concept of self-etching adhesives is based on the use of polymerizable acidic monomers that simultaneously condition and prime dentine and enamel. After dentine demineralisation, mineral ions are removed from the apatite latticework (*i.e.* inorganic matrix), resulting in exposure of the collagen matrix (mainly type I collagen fibrils) (Xu and Wang, 2011). To achieve a thorough wetting of this moist substrate, the use of hydrophilic adhesive components will be necessary. The most widely used self-etching adhesive systems involve two application steps: the conditioning of dentine with a self-etching primer, followed by the application of an adhesive resin (Moszner et al., 2005). Decalcification or conditioning of dentine is an ionic process. Calcium ions are chelated by acidic monomers, and zones of collagen fibres are solubilized or hybridized, as a part of the hybrid complex (Tay and Pashley, 2001). For these ionic processes water is required, and therefore, self-etching adhesives or primers are generally water based

(Moszner et al., 2005). Most of the currently available self-etching primers/adhesives are methacrylate-based with a pH-value in the range of 1.5-2.5. Under these strong acidic conditions, esters such as methacryloyloxydecyl dihydrogen phosphate (MDP) or 2-hydroxyethyl methacrylate (HEMA), both present in the Clearfil SE Bond (SEB) chemical formulation, are hydrolytically degraded (Salz et al., 2005). The non-impregnated demineralised dentine which results after an insufficient resin infiltration or after solubilization and hydrolytic degradation of the resin (Salz et al., 2005), at the hybrid layer (HL) or at the bottom of the hybrid layer (BHL) is the weakest zone within the adhesive interface (De Munck et al., 2005). This unprotected and weak resin-dentine interface remains susceptible to the proteolytic activity of the host-derived matrix-metalloproteinases (MMPs) enzymes (Osorio et al., 2011a), overtime. Thereby, the bonded interface at dentine remains the Achilles' heel of dental restorations (Oguri et al., 2012).

The use of self-etching agents eliminate the conditioning, rinsing and drying steps, typical of etch-and-rinse adhesives (Moszner et al., 2005). Thereby, treatment with SEB dissolved, not removed, the mineral content of both smear layer and superficial dentine after applying acidic components (Dieng-Sarr et al., 2011; Takatsuka et al., 2005). Therefore, mineral crystallites remaining within the collagen after partial demineralisation might act as seed sites for further apatite growth (Bertassoni et al., 2010). Those minerals come from the dissolved and etched smear layer and superficial dentine. The existence of these crystals can induce and facilitate further dentine remineralisation (Saito et al.,1998). Those nucleating demineralised surface might promote structural and compositional changes that would enable the denser packing of the clusters and their subsequent fusion to form amorphous calcium phosphate and ultimately apatite crystals (Saito et al., 1998; Veis and Dorvee, 2013). However,

achieving remineralisation of dentine remains one of the most difficult tasks in dentistry (Bertassoni et al., 2010; Takatsuka et al., 2005). The chemical structure of MDP has been proven to play a key role in both the initial bonding performance as well as the durability of the adhesive interface (Inoue et al., 2005; Toledano et al., 2007; Van Meerbeek et al., 2011). The quality and the longevity of the resin-dentine interface may be increased by using innovative dental adhesives containing zinc within their composition, as Zn-doped adhesives have been shown to induce collagen-stabilization against MMPs degradation (Osorio et al., 2011b; Osorio et al., 2012), preserving the integrity at the resin-dentine interface. Zinc may not only act as a MMPs inhibitor, but it may also influence signaling pathways and stimulate a metabolic effect in hard tissue mineralisation (Hoppe et al., 2011). It may also be that effective inhibitors of MMPs included in resin-dentine bonding interfaces may protect the seed crystallite-sparse collagen fibrils of the scaffold from degradation, allowing them to become remineralised (Liu et al., 2011). Zinc has also been shown to inhibit dentine demineralisation (Takatsuka et al., 2005). These effects make zinc attractive for use as therapeutic agent in the fields of hard and soft tissue engineering. *In vitro* effects of mechanical stimuli have promoted remineralisation at the resin-dentine interface (Toledano et al, 2014a). The experimental clinical exploitation of combining Zn-doped self-etching dentine adhesives, as innovative bioactive ion-releasing restorative materials, and mechanical loading to achieve therapeutic effects on the mineral depleted sites, within the bonded-dentine interface, might result promising. This would provide better insights and therapeutic approaches for management of dental disease.

The purpose of this study was to assess the resin-dentine bond strength and the ability of a two-steps self-etching dental adhesive doped with zinc at the primer or at the bonding components to induce remineralisation at the bonded dentine interface, and after *in vitro*

mechanical loading. This study tested the two null hypotheses that, 1) functional remineralisation of dentine interface obtained with zinc-doped self-etching adhesives at both primer *vs* bond components is neither produced nor influenced by load application, and 2) load cycling has no effect on the microtensile bond strength (BS) of samples bonded with zinc-doped self-etching adhesives to sound dentine.

2.- MATERIAL AND METHODS

2.1. Specimen preparation, bonding procedures and mechanical loading.

Human molars extracted for surgical reasons were obtained with informed consent from donors (20–40 year of age), under a protocol approved by the Institution Review Board. Molars were stored at 4ºC in 0.5% chloramine T for up to 1 month before use. A flat mid-coronal dentine surface was exposed using a hard tissue microtome (Accutom-50; Struers, Copenhagem, Denmark) equipped with a slow-speed, water-cooled diamond wafering saw (330-CA RS-70300, Struers, Copenhagen, Denmark). A 180-grit silicon carbide (SiC) abrasive paper mounted on a water-cooled polishing machine (LaboPol-4, Struers, Copenhagem, Denmark) was used to produce a clinically relevant smear layer (Koibuchi et al., 2001).

A two-step self-etching system, Clearfil SE Bond (Kuraray, Tokyo, Japan) (Clearfil SE) was tested. It was zinc doped by mixing the primer of SEB (SEB·P) with 10 wt% ZnO microparticles (1 to 2 microns) (Panreac Química, Barcelona, Spain) were added to the primer of SEB (SEB·P) (SEB·P-ZnO) or to the bonding resin (SEB·Bd) (SEB·Bd-ZnO); or 2 wt% of $ZnCl_2$ crystals (Sigma Aldrich, St. Louis,MO, USA) were actively dissolved into the primer (SEB·P) (SEB·P-$ZnCl_2$) or into the bonding resin (SEB·Bd) (SEB·Bd-$ZnCl_2$). To achieve complete dissolution of $ZnCl_2$ and dispersion of ZnO particles, adhesive blends were vigorously shaken 1 min in a tube agitator (Vortex

Wizard 51075; Velp Scientifica, Milan, Italy). The complete process was performed in the dark. Preparation of the adhesives and zinc concentrations were based upon previous studies (Osorio et al., 2011b; Toledano et al., 2012a; Toledano et al., 2013). The chemical and descriptions of the adhesives are provided in Table 1.

The specimens were divided into the following main groups based on the tested adhesive systems: (i) Group SEB: Clearfil SEB; (ii) Group SEB·P-ZnO: SEB·P-ZnO was applied followed by the resin bonding (SEB·Bd); (iii) Group SEB·P-$ZnCl_2$: SEB·P-$ZnCl_2$ was applied followed by de resin bonding (SEB·Bd); (iv) Group SEB·Bd-ZnO: SEB·Bd-ZnO was applied after the primer (SEB·P) placement, and (v) Group CSEB·Bd-$ZnCl_2$: CSEB·Bd-$ZnCl_2$ was applied after the primer (SEB·P) placement. The bonding procedures were performed in moist dentine following the manufacturer´s instructions. Excess dentine moisture was removed using absorbent paper, leaving the dentine wet (Faria-e-Silva et al., 2013). A flowable resin composite (X-FlowTM, Dentsply, Caulk, UK) was placed incrementally in five 1 mm layer and light-cured with a Translux EC halogen unit (Kulzer GmbH, Bereich Dental, Wehrheim, Germany) for 40 s. Half of the teeth were stored for 24 h in simulated body fluid solution (SBF) (Osorio and Toledano, 2014; Toledano et al., 2014a), and the other half were mounted in plastic rings with dental stone for load cycling, in SBF (100,000 cycles, 3 Hz, 49 N). This compressive load was applied to the flat resin composite buildups using a 5-mm-diameter spherical stainless plunger, attached to a cyclic loading machine (S-MMT-250NB; Shimadzu, Tokyo, Japan) (Toledano et al., 2014a). The rest of the time until complete 24 h, the loaded specimens were kept in SBF, at 37 ºC.

2.2. Microtensile Bond Strength

Four teeth from each group were sectioned into serial slabs, and further into beams with cross-sectioned areas of 1 mm^2. Specimens were attached to a modified Bencor Multi-T

testing apparatus (Danville Engineering Co., Danville, CA) with a cyanoacrylate adhesive (Zapit/Dental Venture of America Inc., Corona, CA, USA). Then, they were stressed to failure in tension (Instron 4411 /Instron Inc., Canton, MA, USA) at a crosshead speed of 0.5 mm/min. The cross-sectional area at the site of failure of the fractured specimens was measured to the nearest 0.01mm with a pair of digital calipers (Sylvac Ultra-Call III, Fowler Co Inc., Newton, Mass, USA). Bond strength values were calculated in MPa.

Fractured specimens were examined with a stereomicroscope (Olympus SZ-CTV, Olympus, Tokyo, Japan) at 40x magnification to determine the mode of failure. Failure modes were classified as adhesive or mixed.

2.3. FESEM and EDX analysis.

Representative specimens of each group were fixed in a solution of 2.5% glutaraldehyde in 0.1 mol/L sodium cacodylate buffer for 24 h, rinsed three times in 0.1 mol/L sodium cacodylate buffer. Samples were placed in an apparatus for critical point drying (Leica EM CPD 300, Wien, Austria). They were, then, sputter-coated with carbon by means of a sputter-coating Nanotech Polaron-SEMPREP2 (Polaron Equipment Ltd., Watford, UK) and observed with a field emission scanning electron microscope (FESEM Gemini, Carl Zeiss, Oberkochen, Germany) at an accelerating voltage of 3 kV. Energy-dispersive analysis was performed in selected points using an X-ray detector system (EDX Inca 300, Oxford Instruments, Oxford, UK) attached to the FESEM. MTBS values were analyzed by two-way ANOVA (independent factors are mechanical loading and adhesive type) and Student Newman Keuls multiple comparisons tests. For all tests, statistical significance was set at a = 0.05.

2.4. AFM imaging and nano-indentation.

Thirty bonded interfaces were used for the test. An atomic force microscope (AFM – Nanoscope V, Digital Instruments, Veeco Metrology group, Santa Barbara, CA, USA) equipped with a Triboscope indentor system (Hysitron Inc., Minneapolis, MN, USA) and a Berkovich indenter (tip radius 20 nm) was employed for the indentation process in a fully hydrated status (Sauro et al., 2012). For each subgroup, three slabs were tested. On each slab, five indentation lines were executed in five different mesio-distal positions along the interface in a straight line starting from the adhesive layer down to the intertubular dentine. Indentations were performed with a load of 4000 nN and a time function of 10 s. The distance between each indentation was kept constant by adjusting the distance intervals in 1.5 (±1) μm steps (Toledano et al., 2013). Modulus of elasticity (Ei) data were registered in GPa. Data were analyzed by two-way ANOVA (independent factors were mechanical loading and adhesive type) and Student–Newman–Keuls multiple comparisons ($P < 0.05$).

2.5. Raman spectroscopy and cluster analysis.

A dispersive Raman spectrometer/microscope (Horiba Scientific Xplora, Villeneuve d´Ascq, France) was also used to analyze bonded interfaces. The checking protocol for autocalibration procedure was undertaken before each analysis, regularly, using the 521 cm^{-1} line of Si in a silicon wafer. Focus was applied on it, using a 100x magnification objective. Then, the diffraction grating drop down to calibrate (600T) and the reference laser from the laser drop down were selected. Other parameters used in the data acquisition (Slit=100; Hole=300; Filter 50%) were incorporated into the program for the analysis. A 785-nm diode laser (100 mW sample power) through a X100/0.90 NA air objective was employed. Raman signal was acquired using a 600-lines/mm grating centered between 900 and 1,800 cm^{-1}. Chemical mapping of the interfaces was performed. For each specimen a 45 μm x 45 μm area of the interfaces was mapped

using 2 μm spacing at X axis and 1 μm at Y axis. Chemical mapping was submitted to K-means cluster (KMC) analysis using the multivariate analysis tool (ISys® Horiba), which includes statistical pattern to derive the independent clusters. Hypotheses concerning the number of clusters formed in resin-bonded interfaces were previously obtained (Toledano et al., 2015, 2014b). However, Ward's method was employed to get some sense of the number of clusters and the way they merge as seen from the dendrogram. The aim of a factor analysis lies in the effective reduction of the dataset dimension while maintaining a maximum of information. This method was used to model the data and to determine spectral variances associated for data differentiation. It resulted in the calculation of a new coordinate system whereby variations of the dataset is described via new axes, principal components (PC). The K-means clustering is a method of cluster analysis based on a centroid model which aims to partition *n* observations into *k* clusters in which each observation belongs to the cluster with the nearest mean (Almahdy et al., 2012). The natural groups of components (or *data*) based on some similarity and the centroids of a group of *data* sets were found by the clustering algorithm once calculated by the software. To determine cluster membership, this algorithm evaluated the distance between a point and the cluster centroids. The output from a clustering algorithm was basically a statistical description of the cluster centroids with the number of components in each cluster. The biochemical content of each cluster was analyzed using the average cluster spectra. Four clusters were identified and values for each cluster such as adhesive, hybrid layer, bottom of hybrid layer and dentine, within the interface, were independently obtained. Principal component analysis (PCA) decomposed *data* set into a bilinear model of linear independent variables, the so-called principal components (PC_S). Two principal components were selected for the present study at the interfaces: hybrid layer (HL) and

bottom of hybrid layer (BHL). The observed spectra were described at 900-1800 cm^{-1} with 10 complete overlapping Gaussian lines, suggesting homogeneous data for further calculations (Nakabayashi, 1992; Ager et al., 2005). A comparison of the spectra that were collected from the two specimens which compose each subgroup indicated complete overlap, suggesting similarity between both measurements.

The mineral component of dentine, at both HL and BHL was analyzed as follows (Toledano et al., 2014a):

Relative presence of mineral:

1. *Phosphate* (960 cm^{-1}) *and carbonate* (1070 cm^{-1}) *peaks and areas of their bands.* Peak heights were processed in absorbance units.
2. *Relative mineral concentration* (RMC) (*i.e.*, mineral-to-matrix ratio): It was inferred from the visible ratio of the intensities of the peaks at 960 cm^{-1} (phosphate) (PO_4^{3-}) and 1003 cm^{-1} (phenyl group), the aromatic ring of phenylalanine residues in collagen. These indexes concerned with the maximum relative degree of mineralization (Schwartz et al., 2012; Karan et al., 2009)**.** Additionally, peaks at 960 cm^{-1} and 1450 (CH_2) or 1070 cm^{-1} and 1450 can be used (Wang et al., 2009).

Crystallinity: It was evaluated based on the full width at half maximum (FWHM) of the phosphate band at 960 cm^{-1} and carbonate band at 1070 cm^{-1}. These indexes expressed the crystallographic or relative atomic order, since narrower peaks suggest less structural variation in bond distances and angles (Schwartz et al., 2012). In general, the narrower the spectral peak width is, the higher the degree of mineral crystallinity (Karan et al., 2009).

Gradient in mineral content (GMC), or carbonate content of the mineral crystallites: It was assessed as the relationship between the ratio of heights at 1070 cm^{-1} (carbonate)

(CO_3^{2-}) to 960 cm^{-1} (phosphate) (PO_4^{3-}), indicating carbonate substitution for phosphate (Schwartz et al., 2012).

Phosphate peaks ratio (PPR): it assesses the ratio between the mineral peak at 960 cm^{-1} (phosphate) (PO_4^{3-}), within the demineralised zone and the mineral peak (PO_4^{3-}) within the healthy substratum (Milly et al., 2014).

The organic component of dentine was analyzed examining the following parameters:

Normalization: Phenyl group: The peak at 1003 cm^{-1}, which is assigned to C-C bond in the phenyl group, was used for normalization (Xu and Wang, 2011).

Crosslinking:

1. Pyridinium ring vibration: In the spectra, the peak appeared at 1030/1032.7 cm^{-1}, is assigned to the C-C in pyridinium ring vibration which has a trivalent amino acid crosslinking residue (Daood et al., 2013). The relative intensity of this peak increases after the crosslinking formation (Jastrzebska et al., 2003).
2. Ratio Pyridinium/Phenyl (1032 cm^{-1}/1001 cm^{-1}): the higher the ratio, the greater the extent of collagen cross-linking (Jastrzebska et al., 2003; Xu and Wang, 2012).
3. Ratio 1003 (phenyl)/1450 (CH_2): arises preceding deposition of HAP (hydroxyapatite) crystals within the structure (Wang et al., 2009).
4. AGEs (advance glycation end products)-pentosidine at 1550 cm^{-1}, interpreted as a marker of the aging process (Sell and Monnier, 1989).

Nature of collagen:

1. Amide III, CH_2 and amide I: The peaks at 1246/1270, 1450 and 1655/1667 cm^{-1} , assigned to amide III, CH_2 and amide I, respectively, are sensitive to the molecular conformation of the polypeptide chains (Xu and Wang, 2011;

Jastrzebska et al., 2003). The decrease of amide I peak indicates damage or removal of collagen fibrils (Xu and Wang, 2012).

2. Ratio amide I/amide III concerned the organization of collagen.
3. Ratio amide III /CH_2 wagging mode indicates the structural differences (Salehi et al., 2013).
4. Ratio amide I/CH_2 indicates altered collagen quality (Salehi et al., 2013).
5. Ratios amide III and I/AGEs-Pentosidine, indicatives of the glycation reaction *vs* collagen scaffolding (Salehi et al., 2013).
6. 1340 cm^{-1} peak: This signal has been assigned to protein α-helices where intensity is sensitive to molecular orientation (Wang et al., 2009).

Degree of adhesive presence:

1. *Degree of conversion of adhesive*: Ratio 1637/1608. The peak appearing at 1637 cm^{-1} is associated with C=C of methacrylate, and the peak at 1608 cm^{-1} is related to C-C in phenyl of the adhesive monomer (Xu and Wang, 2012).
2. *Bis-GMA penetration*: Ratio1113/1667. The peak appearing at 1113 cm^{-1} is associated with C-O-C of the adhesive, and the peak at 1667 cm^{-1} is related to amide I (Wang and Spencer, 2003; Xu and Wang, 2012).
3. *Adhesive (Bis-GMA and HEMA) penetration*: Ratio1454/1667. The peak appearing at 1454 cm^{-1} is assigned to the CH_2 group of both Bis-GMA and HEMA, and the peak at 1667 cm^{-1} is related to amide I (Wang and Spencer 2003; Xu and Wang, 2012).
4. *Others*: The peak at 1720 cm^{-1} is associated with carbonyl group. The peak at 1453 cm^{-1} is associated at CH_2 def (Wang and Spencer; 2003, Xu and Wang, 2012).

2.6. Light microscopy–Masson's trichrome staining.

Three resin-dentine bonded slices from each group were used for the histo-morphological evaluations. The medial aspects of each resin-dentine bonded slice was fixed in a glass holder with a photo curing adhesive (Technovit 7210 VLC, Heraeus KulzerGmbH Co., Werheim, Germany). Then, they were grounded with SiC papers of increasing fine grits (800, 1000, 1200 and 4000) in a polisher (Exakt, Apparatebau D-2000, Norderstedt, Germany) until its thickness was approximately 10 mm. Slices were stained with Masson's trichrome for differentiation of resin and non-resin encapsulation of the exposed collagen. This dye has a high affinity for cationic elements of normally mineralised type I collagen, resulting in staining collagen green, and when demineralised, resulting in different coloration, generally red; collagen coated with adhesive stains orange and pure adhesive appears beige. Slices with adherent stained sections were dehydrated through ascending ethanol and xylene. The sections were cover slipped and examined by light microscopy (BH-2, Olympus, Tokyo, Japan) at 100× magnifications. Three slices were prepared from each specimen, and images were digitalized in a scanner (Agfa Twin 1200, Agfa-Gevaert NV Mortsel, Belgium). In each specimen, the presence or absence of a red band (that would correspond to demineralised dentine) was observed. A qualitative assessment of the collagen encapsulation was completed by observing color differences within the interfacial zones of resin-dentine interfaces (Toledano et al., 2012b).

3. RESULTS AND DISCUSSION.

Attained nanomechanical properties (Ei) for each group are displayed in Figure 1, and Raman spectroscopy -cluster analysis of the resin-dentin interface in Figures 2 and 3. Light micrographs (Masson's trichrome) and FESEM-EDX images are displayed in Figures 4 and

5, respectively. Table 1 describes the materials and chemical used for the study. Tables 2 and 3 represent microtensile bond strength (MTBS) results (mean and standard deviation), and Raman peaks intensities/ratios of mineral, organic and adhesive components at the resin-dentin interface, respectively.

The null hypothesis that load cycling has no effect on the microtensile bond strength (BS) of samples bonded with zinc-doped self-etching adhesives to sound dentine must be reconsidered, as mechanical loading did not influence bond strength results, but increased the percentage of adhesive failures. Indeed, occlusal function or *in vitro* mechanical loading have been identified as a significant factor to the age of restorations at failure. Such an influence might simply be due to fatigue of the interface where cyclic stresses transmitted across the adhesive and hybrid layers accelerate degradation of the interface. It has been pointed out that fatigue stress (Nikaido et al., 2002) produces a failure mostly at the top or beneath the HL where demineralised collagen fibrils were exposed and the adhesive failed to envelop the collagen network properly (Prati et al., 1999; Toledano et al., 2006). Thus, cycling loading lowered, in general, the resin-dentine bond strength of the adhesives to dentine (Toledano et al., 2006) and in the air-dried smear layer-covered dentine when self-etching adhesives were used; nevertheless, load cycling did not affect bond strength results when a hydrated smear layer was used as substrate for self-etching adhesives (Osorio et al., 2005) or when EDTA-treated dentine surfaces were resin-infiltrated with an etch-and-rinse adhesive zinc-doped or not (Toledano et al., 2015). Even more, EDTA-treated specimens bonded with experimental resins, showed no significant difference in bond strength after load cycling (Sauro et al., 2011). Apart from our previous results, some other author neither obtained bond strength increase after load cycling (Nikaido et al., 2002; Feitosa et al., 2014).

All Zn-doped samples, except SEB·P-$Zncl_2$, performed similar when load cycling was not applied on restored teeth. After mechanical loading, SEB·P-$ZnCl_2$ attained the lowest bond strength values and higher percentage of mixed failures; the rest of specimens performed similar (Table 2). Two main factors explain the attained higher bond strength: (i) the low-dissolution rate of MDP calcium salts that were formed through the creation of strong ionic bonds (Yoshida et al., 2004); and (ii) the very effective polymerization of this adhesive system (Nunes et al., 2005). Functional phosphate monomers have been known for a long time in adhesive dentistry; phosphoric acid monomers such as 10-methacryloyloxydecyl dihydrogen phosphate (MDP) may have a potential for chemical bonding to calcium ions (Yoshida et al., 2004). The reasoning for the general reliability in bonding efficacy by using SEB and SEB Zn-doped adhesive resins may be explained by the chemical stability of MDP-Ca salts (Yoshida et al., 2004), since the long apolar decyl-group renders MDP rather hydrophobic. According to the adhesion–decalcification concept (Yoshida et al., 2004; Van Meerbeek et al., 2011), monomers that etch rather than chemically interact with calcium ions attain lower chemical bonding effectiveness to dentine. Monomers having weak interaction with hydroxyapatite are less prone to produce high initial bond strength and durability, compared with those with a higher chemical interaction (Van Landuyt et al., 2008). Additionally, load cycling gave rise to the increase in the percentage of adhesive over mixed failures (Table 2). Fatigue stress produces a failure mostly at the top or beneath the HL where demineralised collagen fibrils were exposed and the adhesive failed to envelop the collagen network properly (Nikaido et al., 2002; Prati et al., 1999).

The lower percentage distribution of mixed failures after mechanical loading may be related to the increase in mineral precipitation which strengthens the interface. It also

may be associated to some changes in either organic and adhesive components at the resin-dentine interface, affecting both the hybrid layer (HL) and bottom of hybrid layer (BHL), as Raman analysis showed (Table 3). When SEB·P-ZnO was applied on dentine and then load cycled, the degree of mineralization related to both phosphate (960 cm^{-1}) and carbonate (1070 cm^{-1}) height of peaks were higher than in the unloaded specimens, at hybrid layer (HL) [~2.03 fold in phosphate (PO^{3-}_4) and ~1.39 fold in carbonate (CO^{2-}_3)] and bottom of the hybrid layer (BHL) (~1.08 fold in phosphate and ~1.03 fold in carbonate) (Table 3a) (Figs 2DI, 2DII). The presence of a prominent carbonate band around 1070 cm^{-1} (Table 3a) (Fig 3B) is significant because it shows the degree of carbonate substitution in the lattice structure of apatite (Salehi et al., 2013). This increment in the relative presence of mineral, after loading SEB·P-ZnO samples, corresponded with *i)* an increase of ~1.34 fold in the relative mineral concentration (RMC) between phosphate and phenyl (1003 cm^{-1}), the aromatic ring of phenylalanine residues in collagen (Schwartz et al., 2012), and *ii)* an increase in crystallographic perfection in the apatite unit cell, *i.e.,* lower FWHM, which was evidenced in Table 3A and Fig 3B. Additionally, *iii)* the gradient of mineral content (GMC) was lower (~1.45 and ~1.06 at HL and BHL, respectively), and the phosphate peaks ratio was higher (~2 and ~1.07 at HL and BHL, respectively) after load cycling (Table 2a). The lower carbonate substitution for phosphate, plus the higher phosphate peak ratio evokes the presence of advanced apatite maturity (Schwartz et al., 2012; Milly et al., 2014). Field emission scanning electron microscopy confirmed the presence of new mineral formation at both intertubular and peritubular dentine (Fig 5D). The EDX analysis revealed the formation of phosphate deposits, promoted by the Zn-doped MPD monomers, principally formed by zinc phosphates (Feitosa VP et al., 2014). This

augmented precipitation of minerals *vs* absence of unprotected and demineralised collagen layer were noticed at the resin-dentine interface of specimens treated with SEB·P-ZnO after load cycling (Fig 4D). A previous narrow purple-red line representing mild collagen demineralisation was detectable below the thin orange-stained hybrid layer in the SEB·P-ZnO unloaded specimens (Fig 4C), though FESEM analysis confirmed the presence of mineral precipitates on dentine structures (Fig 5C), higher than in SEB unloaded (Fig 5A). In general, specimens treated with SEB·P-$ZnCl_2$ showed, at both HL and BHL, lower intensity bands at both phosphate peak and area, denoting less presence of this mineral (Figs 2EI, 2EII). Nevertheless, these new crystals were less mature than the ones promoted after SEB·P-ZnO dentine application, as FWHM and GMC were higher when zinc chloride was combined with SEB primer (SEB·P) (Table 3a). This diminution of the relative presence of minerals match with the lower bond strength and percentage of mixed failures that were attained (Table 2). It also coincides with some non-uniform purple and red areas below the adhesive interface, representative of the advanced demineralisation front within the resin-dentine interface. This Masson's trichrome light micrographs (Fig 4E) denoted the existence of a partially demineralised layer at the bottom of the hybrid layer. Nevertheless, FESEM analysis permitted to observe multiple mineral formations emerging from the resin-dentine infiltrated layer, trying to occlude the entrance of tubules (Fig 5 E). SEB·P-$ZnCl_2$ load cycled, on the contrary, produced minimal dentine demineralisation (Fig 4F). This mineral growth made disappear the wide and intense red staining layer, indicating that the partially demineralised fringe at the hybrid layer became remineralised after mechanical loadin; this was confirmed in Fig 5F, which showed multi-layered platform of crystals of Zn-based crystals, as denoted the EDX analysis. Dentine treated with both SEB·Bd-ZnO and SEB·Bd-$ZnCl_2$ showed lower height of

phosphate (Figs 2H, 2J) and carbonate peaks after load cycling (~1.01 and ~2.93, respectively), in comparison to the unloaded specimens (Fig 3C); the area of phosphate followed similar trend. In addition, the light microscopy evaluation confirmed this relative lack of mineral, as some non uniform and discontinuous zones of the interface exhibited redder areas below the adhesive layer. These Masson's trichrome-stained sections (Figs 4H, 4J) evidenced the partial demineralisation and the exposed proteins at the resin-dentine interface. These findings were compatible with other mechanical loading outcomes, which not only originated an increase of the gradient in mineral content (GMC), but these crystals showed higher crystallinity (lower FWHM) and lower GMC ratio when SEB·Bd-ZnO was used (Table 3a) (Fig 3C). Nevertheless, specimens treated with SEB·Bd-$ZnCl_2$ showed an increase in GMC ratio. The phosphate Raman peaks intensities have been reported as a suitable parameter to detect differences between intact and demineralised substratum regions (Milly et al., 2014). The ratio phosphate peak/healthy substratum (PPR) showed higher values after cycling loading when ZnO was used as doping agent, concurring with the global increase of relative presence of minerals which attained these doped groups (Table 3a). These new minerals organized in a dense network of plate-like multilayered crystals, forming multiple cavities and hollows throughout the whole resin-dentine interface (Fig 5H). On the contrary, specimens doped with $ZnCl_2$ (either SEB·P or SEB·Bd) showed the lowest PPR, at resin-dentine interfaces (Table 3a), though intertubular and peritubular dentine appeared strongly mineralised (Fig 5J). These crystals appeared as amorphous clumps of buttons-like materials, whose nature probably is phosphate complexes due to the reaction of MPD, Zn^{++} and Ca^{++} during the application of Zn-doped MPD solution on a calcium-rich dentine surface (Feitosa VP et al., 2014).

Concerning the organic components in dentine, load cycling increased collagen crosslinking at the interface of dentine treated with both SEB·P-ZnO and SEB·P-$ZnCl_2$, as the peaks at 1032 cm^{-1} (pyridinium) and 1550 (AGES-Pentosidine), and the ratios 1031/1001 cm^{-1} and 1003/1450 cm^{-1}, increased in their intensities (Table 3b) (Fig 3B). Pyridinium ring decreased its intensity, after loading, in the SEB·P-$ZnCl_2$ group, matching with a lower Ei, in comparison to SEB·P-ZnO (Fig 1). A decrease in pyridinium crosslinks has been previously associated with a wide reduction of bending strength and modulus of cortical bone (Oxlund et al., 1995). Pyridinium was formed within the N- and C-terminal telopeptides. This enzymatic modification is initiated by the oxidation of lysine and hydroxylysine residues that are catalyzed by the enzyme lysyl oxidase (Garnero, 2012). Pentosidine is a crosslinking AGE (advance glycation end products), which is likely to be formed between helical lysine and arginine residues of two collagen molecules. The first step in crosslinking AGEs is the reaction of the aldehyde of an open-chain form of glucose with the ε-amino group of collagen-bound lysine to form a glycosyl-lysine via Schiff's base formation (Garnero, 2012). When the bonding of SEB was Zn-doped (SEB·Bd-ZnO or SEB·Bd-$ZnCl_2$), the whole indexes reflected a crosslinking decreased after mechanical loading, except the ratio 1031/1001 which gave rise to an increase in intensity values (Table 3b). The ratios which evoke the nature of collagen *i.e.,* A-III (1246-1270 cm^{-1}), A-I (1655-1667 cm^{-1}), Ratios Amide I/A-III, A-III and I/CH_2, A-III and I/AGES-Pentosidine, and α-helices (Fig 3C) increased at both HL and BHL after load cycling (Table 3b). This increases indicate recovery (Xu and Wang, 2012), better organization (Toledano et al., 2014a), improved structural differences and collagen quality (Salehi et al., 2013), when SEB·P-ZnO was applied on dentine and then cycled (Table 3b) (Fig 3B). It also denotes a greater sensitivity to molecular orientation in order to enhance further crystallization (Wang et

al., 2009), as mineral nucleation is more advanced in comparison with the SEB·P-$ZnCl_2$ group (Table 3a). Some studies performed on other hard tissues (bone) have determined that higher AGE content may be associated with denser and more complex rod-like trabecular architecture. This also depends on local bone tissue maturation and it affects not only the bone toughness but also the stiffness, and the elastic modulus independent of the mineral phase (Garnero, 2012). The increase of collagen maturation has been also associated with a dose-dependent increase of pentosidine that was correlated with bone turnover rate (Saito et al., 2008). Tang et al., (2010) have stated that an increase of AGE crosslink induces a marked decrease in the propagation fracture toughness, in bone. SEB·P-$ZnCl_2$, on the contrary, showed in general a worst molecular conformation (A-III, CH_2, A-I), collagen scaffolding (A-III and I/AGES-Pentosidine) and orientation (α-helices) (Fig 3B). These findings are in line with the lower bond strength (Table 2), relative presence of minerals (Table 3a) and pyridinium intensity (Table 3b) that were attained when samples were treated with SEB·P-Zn doped. After including Zn into the bonding component of SEB (SEB·Bd), a general decrease of height peaks and ratios concerning the nature of collagen were observed, more intense in the samples which were treated with SEB·Bd-$ZnCl_2$, and then load cycled (Table 3b) (Fig 3C).

Raman analysis only provides quantitative information on the changes in mineral and matrix structures, but this method does not differentiate the contributions of intra- and extrafibrillar mineral. Most importantly, it cannot evaluate the effectiveness of the remineralisation procedure on the mechanical reinforcement and recovery of the mechanical properties of the partially demineralised dentine (Bertassoni et al., 2009). The mechanical properties of dentine depend on the degree and on the quality of the mineralization. Indeed, the extrafibrillar minerals act as a granular material that can withstand load, but in the absence of intrafibrillar mineralization. Intrafibrillar

mineralization is the key factor to ensuring that collagen fibrils have the same high modulus of elasticity and hardness as occurs in natural biomineralised dentine (Balooch et al., 2008). Therefore, the increase of the elastic modulus (Ei) of the partially demineralised collagen is directly related to the precipitation of minerals at the resin-dentine interface has (Li et al., 2012), and more specifically at the intrafibrillar compartment (Bertassoni et al, 2009; Balooch et al., 2008). At the hybrid layer, specimens treated with both SEB·P-ZnO and SEB·P-$ZnCl_2$ attained the lowest Ei among Zn-doped groups, when samples were not cyclic loaded. On the contrary, groups treated with SEB·Bd-ZnO and SEB·Bd-$ZnCl_2$ showed the biggest modulus of Young in the unloaded specimens, where some slight and faint signs of demineralisation permitted to observe the scarce exposed proteins detected (Figs 4G, 4I). This denoted that most of the precipitated mineral was extrafibrillar, *i.e.,* undertaking a non-functional dentine remineralisation (Balooch et al., 2008). At bottom of hybrid layer, samples with both SEB·Bd-ZnO and SEB unload cycled produced the lowest values of Ei. At both the hybrid layer and the bottom of hybrid layer, SEB and SEB·P-ZnO groups showed the highest Ei after cyclic loading. Therefore, the null hypothesis that functional remineralisation of dentine interface obtained with zinc-doped self-etching adhesives at both primer *vs* bond components is not produced neither influenced by load cycling application, must be rejected. Specimens treated with either SEB·Bd-ZnO or SEB·Bd-$ZnCl_2$ attained the lowest modulus of Young among mechanical loaded groups, at both the hybrid layer (HL) and bottom of hybrid layer (BHL) (Fig 1).

The mechanism of bonding of SEB was shown to be based upon submicron micro-mechanical interlocking (Van Meerbeek et al., 2003), supplemented by primary chemical interaction of the functional monomer MDP with HAp that remained around the partially exposed collagen (Yoshida et al., 2004; Fu et al., 2005). Clearfil SE Bond

adhesive system involves a two-step application procedure; SEB·P represents the much more fluid and thus probably more chemically active component of SEB system, which is applied first. Most likely, the primer itself may have produced self-assembled nano-layering (Yoshida et al., 2012), which consists of two MDP molecules with their methacrylate groups directed towards each other and their functional hydrogen phosphate groups directed away from each other; in between the layers calcium salts are deposited and basically hold the layers together. Zn^{++} may causes interaction with MDP forming Zn-MDP complexes when it is combined with the primer (SEB·P-Zn doped) and applied on dentine previous to the adhesive placement (SEB·Bd), reducing the Ca-MDP salts formation (Osorio et al., 2011b). As a consequence, the penetration of free MDP into the partially demineralised dentine is compromised, due to simultaneous formation of MPD-Zn and Ca-MPD-Zn salts rather than MPD-Ca (Feitosa VP et al., 2014). When dentine was treated with any zinc-doped mixture of SEB bonding system (SEB·Bd), remineralisation of the bonding interface below the resin-primed demineralised collagen was not affected by the presence of a previous adhesive layer (SEB·P). These Ca-MDP complexes, organized in nano-layering (Yoshida et al., 2012) did not hamper the inward diffusion of ions, helping for further interactions between the remaining Ca^{++} and Zn^{++} ions, the curable resin matrix containing acidic functional, Zn-MPD and Ca-MPD-Zn complexes, and the partially demineralised collagen. We speculate that the Zn-MDP complexes formed after mixing Zn-compounds with SEB·Bd may have not promoted intrafibrillar remineralisation (lower Ei) after load cycling at the resin-dentine interface due to, *i)* a restricted formation of *in situ* Ca-MDP salts caused by Zn^{++} interactions (Osorio et al., 2011b), and as result lower formation of nano-layering, *ii)* an over-etching effect produced by $ZnCl_2$, as $ZnCl_2$ is highly acidic, soluble, and hydrophilic (Brown, 2006). These findings are in accordance with the

bonding efficacy results, as a lower bond strength was found when SEB·P-$ZnCl_2$ was employed (Table 2), showing an increase of the adhesive failures at the top or within the hybridized complex (Fig 5J).

This lower salt formation, plus the higher alkalinity promoted after mechanical loading (McAllister and Frangos, 1999) could also account for the less effective release of zinc ions at the resin-dentine interface. Nevertheless, this inhibition effect of Zn^{++} is reverted with an increase of calcium concentration; as Ca^{++} ions increase at the demineralised dentine and beneath the resin-dentine interface (Bertassoni et al., 2010) (BHL), new Ca-MDP salts are formed and greater Ei values are produced at the bottom of the hybrid layer (Fig 1). Collagen crosslinking effect (Table 3b) improved mechanical strength and stability of dentine collagen (Xu and Wang, 2012). It permitted the growing of minerals within the demineralised dentine, as three-dimensional structures supporting effective mineralization may be created between intrafibrillar collagen molecules *via* the assemblage of specific cross-link formation that guide proper mineralization (Saito et al., 2006). It has been shown that this local increase of Ca^{++} concentration may inhibit Zn^{++} binding, depending on the relative abundance of these two divalent ions (Rosenberg et al., 1998). The association among the *in situ* release of Zn^{++}, mineral precipitation and *in vitro* load cycling on partially demineralised and infiltrated dentine is supported by the effect of compressive loads on the stimulation of the tissue-nonspecific alkaline phosphatase (McAllister and Frangos 1999), a zinc-metalloenzyme that hydrolyzes a broad range of phosphate monoesters (Price et al., 2009; Posner et al., 1986). At high phosphate concentration, calcium pyrophosphate, calcium phosphate and unstable and non-crystalline amorphous complexes are formed (Cheng and Pritzker, 1983) (Figs 4J, 5J) around the collagen fibrils, keeping the alkaline phosphatase and other enzymes "fossilized" (Van Meerbeek et al., 2001), thus hindering the complete

remineralisation. Nevertheless, extrafibrillar mineralization, *e.g.*, intratubular and intertubular mineral precipitated were also evidenced (Fig 5J). These findings correlate well with the decrease in both heights of phosphate peak and area, height of carbonate peak and an increase of RMC which have been previously stated (Table 3a) (Figs 2HI, 2JI, 3C).

Load cycling gave rise to an increase in the degree of conversion of the adhesive in all groups, at the resin-dentine interface (Table 2c). Therefore, the chemical interaction of MDP with Zn^{++} in Zn-doped adhesives improved after mechanical loading. Specimens treated with SEB·P-ZnO attained higher Bis-GMA penetration at the resin-dentine interface than the dentine samples infiltrated with SEB·P-$ZnCl_2$ when the specimens were load cycled; nevertheless, though Bis-GMA penetrated deeper in SEB·P-$ZnCl_2$ than in SEB·P-ZnO groups. Both Bis-GMA and HEMA penetration were lower after load cycling in comparison with the unloaded specimens when the primer of the adhesive system (SEB·P) was Zn-doped (Table 3c). Load cycling originated the opposite effect at the interface when the bonding of SEB was doped with zinc compounds, as the degree of Bis-GMA and adhesive (Bis-GMA and HEMA) penetration increased when SEB·Bd-$ZnCl_2$, and decrease after using SEB·Bd-ZnO (Table 3c). The possible coordination of the hydroxyl group of HEMA, which penetrated deeper when SEB·Bd-$ZnCl_2$ was used, with the bivalent cation (Zn^{++}) that is present in both the catalytic domain of MMPs and in the tissue-nonspecific alkaline phosphatase (McAllister and Frangos, 1999), has also been suggested as a possible inhibitory effect of both enzymes (Osorio et al., 2011c; Carvalho et al., 2009), decreasing remineralisation ability (Table 3a, 3c). Mechanical loading showed lower height of peaks at both carbonyl group (1720 cm^{-1}) and CH_2 def (1453 cm^{-1}) when

SEB·P and SEB·Bd were ZnO or $ZnCl_2$ doped, except SEB·P-ZnO, which increase the height of peak at 1720 cm^{-1}.

The control of metallic ions release from dental adhesives must be considered as an attractive approach to enhance the biological capability of adhesives for dental tissue engineering. The analysis of the limited literature available indicates that further specific studies on the relationship between the dentine micro-nanostructure and the mechano-chemical properties of zinc-doped adhesives should be determined. In view of the clinical demand on engineered dental tissue, new adhesive/primers formulations including zinc in their composition should be tested. Thereby, further complementary studies are strongly encouraged.

ACKNOWLEDGMENTS.

This work was supported by grant MINECO/FEDER MAT2011-24551 and MAT2014-52036-P.

The authors have no financial affiliation or involvement with any commercial organisation with direct financial interest in the materials discussed in this manuscript. Any other potential conflict of interest is disclosed.

REFERENCES

Almahdy A, Downey FC, Sauro S, Cook RJ, Sherriff M, Richards D, Watson TF, Banerjee A, Festy F. Microbiochemical analysis of carious dentine using Raman and fluorescence spectroscopy. Caries Res 2012; 46: 432-440.

Ager JW, Nalla RK, Breeden KL, Ritchie RO. Deep-ultraviolet Raman spectroscopy study of the effect of aging on human cortical bone. J Biomed Opt 2005; 10: 034012.

Balooch M, Habelitz S, Kinney JH, Marshall SJ, Marshall GW. Mechanical properties of mineralized collagen fibrils as influenced by demineralization. J Struct Biol 2008; 162: 404-410.

Bertassoni LE, Habelitz S, Kinney JH, Marshall SJ, Marshall GW Jr. Biomechanical perspective on the remineralization of dentin. Caries Res 2009; 43:70-77.

Bertassoni LE, Habelitz S, Pugach M, Soares PC, Marshall SJ, Marshall GW Jr. Evaluation of surface structural and mechanical changes following remineralization of dentin. Scanning 2010; 32: 312-319.

Brown ID. The chemical bond in inorganic chemistry: the bond valence model. Oxford: Oxford University Press, 2006.

Cao CY, Mei ML, Li QL, Lo EC, Chu CH. Methods for biomimetic remineralization of human dentine: a systematic review. Int J Mol Sci 2015;16:4615-4627.

Carvalho RV, Ogliari FA, Souza AP, Silva AF, Petzhold CL, Line SR, Piva E, Etges A. 2-hydroxyethyl methacrylate as an inhibitor of matrix metalloproteinase-2. Eur J Oral Sci 2009; 117: 64–67.

Cheng PT, Pritzker KP. Pyrophosphate, phosphate ion interaction: effects on calcium pyrophosphate and calcium hydroxyapatite crystal formation in aqueous solutions. J Rheumatol 1983;10:769-777.

Daood U, Iqbal K, Nitisusanta LI, Fawzy AS. Effect of chitosan/riboflavin modification on resin/dentin interface: spectroscopic and microscopic investigations. J Biomed Mater Res A 2013;101, 1846-1856.

De Munck J, Van Landuyt K, Peumans M, Poitevin A, Lambrechts P, Braem M, Van Meerbeek B. A critical review of the durability of adhesion to tooth tissue:methods and results. J Dent Res 2005; 84:118-132.

Dieng-Sarr F, Sharrock P, Dabsie F, Grégoire G. Modifications of the organic and mineral fractions of dental tissues following conditioning by self-etching adhesives. J Dent 2011; 39:141-147.

Faria-e-Silva AL, Araújo JE, Rocha GP, de Oliveira Ada S, de Moraes RR. Solvent content and dentin bond strengths using water-wet, ethanol-wet and deproteinization bonding techniques. Acta Odontol Scand 2013;71:710-715.

Feitosa SA, Corazza PH, Cesar PF, Bottino MA, Valandro LF. Pressable feldspathic inlays in premolars: effect of cementation strategy and mechanical cycling on the adhesive bond between dentin and restoration. J Adhes Dent 2014;16:147-154.

Feitosa VP, Ogliari FA, Van Meerbeek B, Watson TF, Yoshihara K, Ogliari AO, Sinhoreti MA, Correr AB, Cama G, Sauro S. Can the hydrophilicity of functional monomers affect chemical interaction? J Dent Res 2014; 93:201-206.

Fu B, Sun X, Qian W, Shen Y, Chen R, Hannig M. Evidence of chemical bonding to hydroxyapatite by phosphoric acid esters. Biomaterials 2005; 26: 5104-5110.

Garnero P. The contribution of collagen crosslinks to bone strength. Bonekey Rep 2012 19;1:182.

Hoppe A, Güldal NS, Boccaccini AR. A review of the biological response to ionic dissolution products from bioactive glasses and glass-ceramics. Biomaterials 2011; 32: 2757–2774.

Inoue S, Koshiro K, Yoshida Y, De Munck J, Nagakane K, Suzuki K, Sano H, Van Meerbeek B. Hydrolytic stability of self-etch adhesives bonded to dentin. J Dent Res 2005; 84:1160-1164.

Jastrzebska M, Wrzalik R, Kocot A, Zalewska-Rejdak J, Cwalina B. Raman spectroscopic study of glutaraldehyde-stabilized collagen and pericardium tissue. J Biomater Sci Polym Ed 2003; 14: 185-197.

Karan K, Yao X, Xu C, Wang Y. Chemical profile of the dentin substrate in non-carious cervical lesions. Dent Mater 2009; 25:1205-1212.

Koibuchi H, Yasuda N, Nakabayashi N. Bonding to dentin with a self-etching primer: the effect of smear layers. Dent Mater 2001;17:122-126.

Li Y, Thula TT, Jee S, Perkins SL, Aparicio C, Douglas EP, Gower LB. Biomimetic mineralization of woven bone-like nanocomposites: role of collagen cross-links. Biomacromolecules 2012; 13:49-59.

Liu Y, Mai S, Li N, Yiu CK, Mao J, Pashley DH, Tay FR. Differences between top-down and bottom-up approaches in mineralizing thick, partially-demineralized collagen scaffolds. Acta Biomater 2011; 7:1742–1751.

McAllister TN, Frangos JA. Steady and transient fluid shear stress stimulate NO release in osteoblasts through distinct biochemical pathways. J Bone Miner Res 1999; 14:930-936.

Milly H, Festy F, Watson TF, Thompson I, Banerjee A. Enamel white spot lesions can remineralise using bio-active glass and polyacrylic acid-modified bio-active glass powders. J Dent 2014; 42:158-166.

Moszner N, Salz U, Zimmermann J. Chemical aspects of self-etching enamel-dentin adhesives: a systematic review. Dent Mater 2005; 21:895-910.

Nakabayashi N. The hybrid layer: a resin-dentin composite. Proc. Finn. Dent. Soc. 1992; 88 (Suppl 1): 321-329.

Nikaido T, Kunzelmann KH, Chen H, Ogata M, Harada N, Yamaguchi S, Cox CF, Hickel R, Tagami J. Evaluation of thermal cycling and mechanical loading on bond strength of a self-etching primer system to dentin. Dent Mater 2002;18: 269-275.

Nunes TG, Ceballos L, Osorio R, Toledano M. Spatially resolved photopolymerization kinetics and oxygen inhibition in dental adhesives. Biomaterials 2005; 26:1809–1817.

Oguri M, Yoshida Y, Yoshihara K, Miyauchi T, Nakamura Y, Shimoda S, Hanabusa M, Momoi Y, Van Meerbeek B. Effects of functional monomers and photo-initiators on the degree of conversion of a dental adhesive. Acta Biomater 2012; 8:1928-1934.

Osorio R, Toledano M, Osorio E, Aguilera FS, Tay FR. Effect of load cycling and in vitro degradation on resin-dentin bonds using a self-etching primer. J Biomed Mater Res A 2005;72:399-408.

Osorio R, Yamauti M, Osorio E, Ruiz-Requena ME, Pashley DH, Tay FR, Toledano M. Zinc reduces collagen degradation in demineralized human dentin explants. J Dent 2011a; 39: 148-153.

Osorio R, Yamauti M, Osorio E, Román JS, Toledano M. Zinc-doped dentin adhesive for collagen protection at the hybrid layer. Eur J Oral Sci 2011b;119:401-410.

Osorio R, Yamauti M, Osorio E, Ruiz-Requena ME,Pashley D, Tay F, Toledano M. Effect of dentin etching and chlorhexidine application on metalloproteinase-mediated collagen degradation. Eur J Oral Sci 2011c; 119: 79–85.

Osorio R, Yamauti M, Sauro S, Watson TF, Toledano M. Experimental resin cements containing bioactive fillers reduce matrix metalloproteinase-mediated dentin collagen degradation. J Endod 2012; 38:1227-1332.

Osorio R, Toledano M. Biomaterials for catalysed mineralization of dental hard tissues. 2014. In: Biomineralisation of Biomaterials: Fundamental and applications. Cambridge, United Kingdom: Woodhead Publishing Limited.

Oxlund H, Barckman M, Ortoft G, Andreassen TT. Reduced concentrations of collagen cross-links are associated with reduced strength of bone. Bone 1995;17(4 Suppl):365S-371S.

Pashley DH, Tay FR. Aggressiveness of contemporary self-etching adhesives. Part II: etching effects on unground enamel. Dent Mater 2001;17:430-444.

Posner AS, Blumenthal NC, Boskey AL. Model of aluminum-induced osteomalacia: inhibition of apatite formation and growth. Kidney Int Suppl 1986;18:S17-S19.

Prati C, Chersoni S, Pashley DH. Effect of removal of surface collagen fibrils on resin-dentin bonding. Dent Mater 1999;15:323-331.

Price PA, Toroian D, Chan WS. Tissue-nonspecific alkaline phosphatase is required for the calcification of collagen in serum: a possible mechanism for biomineralization. J Biol Chem 2009; 284:4594-4604.

Rosenberg K, Olsson H, Mörgelin M, Heinegård D. Cartilage oligomeric matrixprotein shows high affinity zinc-dependent interaction with triple helical collagen. J Biol Chem 1998; 273:20397-20403.

Saito M, Fujii K, Marumo K. Degree of mineralization-related collagen crosslinking in the femoral neck cancellous bone in cases of hip fracture and controls. Calcif Tissue Int 2006;79:160-168.

Saito M, Mori S, Mashiba T, Komatsubara S, Marumo K. Collagen maturity, glycation induced-pentosidine, and mineralization are increased following 3-year treatment with incadronate in dogs. Osteoporos Int 2008;19:1343-1354.

Saito T, Yamauchi M, Crenshaw MA. Apatite induction by insoluble dentin collagen. J Bone Miner Res 1998;13:265-270.

Salehi H, Terrer E, Panayotov I, Levallois B, Jacquot B, Tassery H, Cuisinier F. Functional mapping of human sound and carious enamel and dentin with Raman spectroscopy. J Biophotonics 2013; 6:765-774.

Salz U, Zimmermann J, Zeuner F, Moszner N. Hydrolytic stability of self-etching adhesive systems. J Adhes Dent 2005;7:107-116.

Sauro S, Osorio R, Watson TF, Toledano M. Therapeutic effects of novel resin bonding systems containing bioactive glasses on mineral-depleted areas within the bonded-dentine interface. J Mater Sci Mater Med 2012; 23, 1521-1532.

Sauro S, Toledano M, Aguilera FS, Mannocci F, Pashley DH, Tay FR, Watson TF, Osorio R. Resin-dentin bonds to EDTA-treated vs. acid-etched dentin using ethanol wet-bonding. Part II: Effects of mechanical cycling load on microtensile bond strengths. Dent Mater 2011;27:563-572.

Schwartz AG, Pasteris JD, Genin GM, Daulton TL, Thomopoulos S. Mineral distributions at the developing tendon enthesis. PLoS One 2012; 7: e48630.

Sell DR, Monnier VM. Structure elucidation of a senescence cross-link from human extracellular matrix. Implication of pentoses in the aging process. J Biol Chem 1989; 264, 21597-21602.

Takatsuka T, Tanaka K, Iijima Y. Inhibition of dentine demineralization by zinc oxide: in vitro and in situ studies. Dent Mater 2005; 21:1170-1177.

Tang SY, Vashishth D. Non-enzymatic glycation alters microdamage formation in human cancellous bone. Bone 2010; 46:148-154.

Tay FR, Pashley DH. Aggressiveness of contemporary self-etching systems. I: Depth of penetration beyond dentin smear layers. Dent Mater 2001;17:296-308.

Toledano M, Osorio R, de Leonardi G, Rosales-Leal JI, Ceballos L,Cabrerizo-Vilchez MA. Influence of self-etching primer on the resin adhesion to enamel and dentin. Am J Dent 2001;14:205-210.

Toledano M, Osorio R, Albaladejo A, Aguilera FS, Tay FR, Ferrari M. Effect of cyclic loading on the microtensile bond strengths of total-etch and self-etch adhesives. Oper Dent 2006;31:25-32.

Toledano M, Osorio R, Osorio E, Aguilera FS, Yamauti M, Pashley DH, Tay F. Durability of resin-dentin bonds: effects of direct/indirect exposure and storage media. Dent Mater 2007; 23:885-892.

Toledano M, Yamauti M, Ruiz-Requena ME, Osorio R. A ZnO-doped adhesive reduced collagen degradation favouring dentine remineralization. J Dent 2012a;40:756-65.

Toledano M, Cabello I, Yamauti M, Osorio R. Differential resin-dentin bonds created after caries removal with polymer burs. Microsc Microanal 2012b; 18:497-508.

Toledano M, Sauro S, Cabello I, Watson T, Osorio R. A Zn-doped etch-and-rinse adhesive may improve the mechanical properties and the integrity at the bonded-dentin interface. Dent Mater 2013; 29: e142-e152.

Toledano M, Aguilera FS, Sauro S, Cabello I, Osorio E, Osorio R. Load cycling enhances bioactivity at the resin-dentin interface. Dent Mater 2014a; 30:e169-e188.

Toledano M, Osorio E, Aguilera FS, Sauro S, Cabello I, Osorio R. In vitro mechanical stimulation promoted remineralization at the resin/dentin interface. J Mech Behav Biomed Mater 2014b; 30: 61-74.

Toledano M, Aguilera FS, Osorio E, Cabello I, Toledano-Osorio M, Osorio R. Bond strength and bioactivity of Zn-doped dental adhesives promoted by load cycling. Microsc Microanal 2015;21:214-230.

Van Landuyt KL, Yoshida Y, Hirata I, Snauwaert J, De Munck J, Okazaki M, Suzuki K, Lambrechts P, Van Meerbeek B. Influence of the chemical structure of functional monomers on their adhesive performance. J Dent Res 2008; 87:757-761.

Van Meerbeek B, Vargas S, Inoue S, Yoshida Y, Peumans M, Lambrechts P, VanHerle G. Adhesives and cements to promote preservation dentistry. Oper Dent 2001;26:S119-S144.

Van Meerbeek B, De Munck J, Yoshida Y, Inoue S, Vargas M, Vijay P, Van Landuyt K, Lambrechts P, Vanherle G. Buonocore memorial lecture. Adhesion to enamel and dentin: current status and future challenges. Oper Dent 2003; 28: 215-235.

Van Meerbeek B, Yoshihara K, Yoshida Y, Mine A, De Munck J, Van Landuyt KL. State of the art of self-etch adhesives. Dent Mater 2011; 27:17-28.

Veis A, Dorvee JR. Biomineralization mechanisms: a new paradigm for crystal nucleation in organic matrices. Calcif Tissue Int 2013;93:307-315.

Wang Y, Spencer P. Hybridization efficiency of the adhesive/dentin interface with wet bonding. J Dent Res 2003;82:141-145.

Wang C, Wang Y, Huffman NT, Cui C, Yao X, Midura S, Midura RJ, Gorski JP. Confocal laser Raman microspectroscopy of biomineralization foci in UMR 106 osteoblastic cultures reveals temporally synchronized protein changes preceding and accompanying mineral crystal deposition. J Biol Chem 2009; 284: 7100-7113.

Xu C, Wang Y. Cross-linked demineralized dentin maintains its mechanical stability when challenged by bacterial collagenase. J Biomed Mater Res B Appl Biomater 2011; 96: 242-248.

Xu C, Wang Y. Collagen cross linking increases its biodegradation resistance in wet dentin bonding. J Adhes Dent 2012; 14: 11-18.

Yoshida Y, Nagakane K, Fukuda R, Nakayama Y, Okazaki M, Shintani H, Inoue S, Tagawa Y, Suzuki K, De Munck J, Van Meerbeek B. Comparative study on adhesive performance of functional monomers. J Dent Res 2004; 83:454-458.

Yoshida Y, Yoshihara K, Nagaoka N, Hayakawa S, Torii Y, Ogawa T, Osaka A,Meerbeek BV. Self-assembled Nano-layering at the Adhesive interface. J Dent Res 2012; 91:376-381.

FIGURE CAPTIONS

Fig 1: Mean and SD of Young Modulus (Ei) (GPa) measured at the hybrid layers (HL) and bottom of hybrid layer (BHL) in sound dentine. Identical letters indicate no significant differences between unloaded restorations from the different experimental

groups, identical numbers indicate no significant differences between load cycled restorations from the different experimental groups, and * indicate significant differences between unloaded and load cycled restorations from the same experimental group. Abbreviations: SEB: SE-Bond, SEB·P: SE-Bond primer, SEB·Bd: SE-Bond bonding. ZnO, zinc oxide; $ZnCl_2$, zinc chloride.

Fig 2. I: Three-dimensional (3D) micro-Raman map of the phosphate peak (961 cm^{-1}) intensities at the dentine-bonded interface of SEB-treated dentine surfaces, unloaded (left column), or load cycled (right column). At the 3D micro-Raman map, blue represents the lowest peak intensity, while the red represents the highest. II: K-means clustering (KMC) map of the Raman profile of the sample; (A, B) SEB; (C, D) SEB·P-ZnO doped; (E, F) SEB·P-$ZnCl_2$ doped; (G, H) SEB·Bd-ZnO doped; (I, J) SEB·Bd-$ZnCl_2$. Abbreviations: SEB: SE-Bond, SEB·P: SE-Bond primer, SEB·Bd: SE-Bond bonding. ZnO, zinc oxide; $ZnCl_2$, zinc chloride.

Fig 3. Raman *spectra* of principal components (PCs): HL, hybrid layer; BHL, bottom of hybrid layer for each SEB group. A) SEB; BB SEB·P-Zn doped, and C) SEB·Bd-Zn doped. Abbreviations: SEB: SE-Bond, SEB·P: SE-Bond primer, SEB·Bd: SE-Bond bondin. ZnO, zinc oxide; $ZnCl_2$, zinc chloride.

Fig 4. Representative light micrographs of SEB adhesive systems in sound dentine specimens; interfaces stained with Masson's trichrome: mineralised dentine stained green, adhesive stained beige, and exposed protein stained red. Original magnification: 150X. (A): SEB control (unloaded). (B): SEB load cycled. (C): SEB·P-ZnO unloaded. (D): SEB· P-ZnO load cycled. (E): SEB·P-$ZnCl_2$ unloaded. (F): SEB·P-$ZnCl_2$ load

cycled. (G): SEB·Bd-ZnO unloaded. (H): SEB·Bd-ZnO load cycled. (I): SEB·Bd-$ZnCl_2$ unloaded. (J): SEB·Bd-$ZnCl_2$ load cycled. Limited and clear resin uncovered decalcified dentine is shown (asterisk) (A). Evidence of partial demineralisation or exposed protein may be detectable at the resin-dentine interface and tubular area (asterisks) (E, H, J). Slight and faint signs of demineralisation show the scarce exposed proteins detected (arrow) (F,I). No signs of demineralisation or exposed protein (red stain) are detectable at the resin-dentine interface; clear observation of histological remineralisation of the partially demineralised dentine layer is detected (arrows) (B). Absence of unprotected collagen layer is observable in some specimens (pointers) (C, D, G). Abbreviations: SEB: SE-Bond; SEB·P: SE-Bond primer; SEB·Bd: SE-Bond bonding; ZnO, zinc oxide; $ZnCl_2$, zinc chloride.

Fig 5. Field-emission scanning electron microscopy images of failures after bonding and microtensile bond strength testing. (A) SEB unloaded. (B) SEB load cycled. (C) SEB·B-ZnO unloaded. (D) SEB·B-ZnO load cycled. (E) SEB·B-$ZnCl_2$ unloaded. (F) SEB·P-$ZnCl_2$ load cycled. (G) SEB·Bd-ZnO unloaded. (H) SEB·Bd-ZnO load cycled. (I) SEB·Bd-$ZnCl_2$ unloaded. (J) SEB·Bd-$ZnCl_2$ load cycled. Mixed failures and fracture at the bottom of hybrid complex may be observed in SEB unloaded specimens (A). Collagen fibers are clearly observed at the peritubular (PD) and intertubular dentine (ID), appearing partially mineralised (asterisk) or completely demineralised (pointer). The adhesive layer (a) covering the hybrid complex is shown at the top left corner of the image. Some tubules (t) turned up mineral filled (EDX, spectrum 3). SEB load cycled sample (B) showed a mixed failure with the main fracture at the bottom of the hybridized complex. A dense network of fibrils completely mineralised may be observed on intertubular dentine (ID) and covering the peritubular dentine (PD).

Mineral occlusion (EDX, spectrum 6) was detected into the tubule lumen. The prototypical D-periodicity banding of collagen fibrils was observed, in multiple details (pointer). Especial mineral formations were also observed (arrow). SEB·B-ZnO unloaded (C) showed a mixed failure at the bottom of the hybrid complex. Tubules appeared mineral filled (EDX, spectrum 10). Clumps of precipitation of minerals, in strata (asterisk), covered the whole surface of dentine matrix, allowing the visual observation of tubules.

When SEB·B-ZnO load cycled (D) was analyzed, a mixed failure affecting both the top (asterisk) and bottom (pointer) of the hybrid complex was observable. Precipitated crystals appeared round transversally and slightly elongated longitudinally. They nucleated at both intertubular dentine infiltrated with resin, and peritubular dentine. Some tubules appeared empty, but with a totally mineralised wall (arrow). Zinc-based salts [phosphorous (P), calcium (Ca), and zinc (Zn)] were detected in the elemental analysis (EDX, spectrum 11). SEB·B-$ZnCl_2$ unloaded (E) permitted to observe a mixed failure at the bottom of the hybrid complex. Multiple mineral formations are observed emerging through the resin-dentine infiltrated layer (arrow). At both intertubular and peritubular dentine, terminal knob-like structures are exhibited within the collagen fibres. Tubule entrances appeared visible but completely precipitated by minerals (pointer). Espectrum from energy dispersive analysis, attained at zone 21 is showing elemental composition of phosphorous (P) and calcium (Ca). SEB·P-$ZnCl_2$ load cycled (F) showed a mixed failure with the main fracture at the bottom of the hybridized complex. Failure surface analysis permitted to observe multiple strata of mineral precipitations around the tubule wall. Minerals formed a collar around the narrowest ring of the tubule lumen (pointer), detected below the deepest platform of crystals (asterisk). Zinc-based [phosphorous (P), calcium (Ca), and zinc (Zn)] salts were

detected in the elemental analysis (EDX, spectrum 22). SEB·Bd-ZnO unloaded (G) produced a mixed failure, affecting both the adhesive surface (asterisk) and the partially demineralised dentine (arrow) at the bottom of the hybrid complex. Mineralised dentine collagen without resin infiltration was detected inside the tubule wall, where crystals precipitated in knob-like formations (arrow). Multiple collagen fibrils appeared longitudinally mineralised (pointer). Espectrum from energy dispersive analysis, attained at zone 26, is showing elemental composition of phosphorous (P), calcium (Ca), and zinc (Zn). After using SEB·Bd-ZnO load cycled (H), a mixed failure was present. Both infiltrated (asterisk) and remineralised dentine (arrow) are involved. Mineral precipitates throughout the dense network of plate-like multilayered crystals on the dentine surface were shown. An extensive labyrinth of reticular mineral depositions, cavities and hollows made of resin and mineral were perceptible (pointer). Phosphorous (P) and calcium (Ca) were detected in the elemental analysis (EDX, spectrum 18). SEB·Bd-$ZnCl_2$ unloaded specimens (I) originated a mixed failure at the top of the hybrid complex. A mineral deposition is completely covering the dentine surface. This substratum resulted completely mineralised and the mineral formations only allowed a restricted display of the tubule entrances (asterisks). The typical staggered pattern of collagen fibrils due to the characteristic D- periodicity (67 nm) was visible at the fibers which cover the intertubular dentine (arrows). Espectrum from energy dispersive analysis, attained at zone 27, is showing elemental composition of phosphorous (P), calcium (Ca), and zinc (Zn). (J) SEB·Bd-$ZnCl_2$ load cycled specimens showed a mixed failure with the main fracture at the top of the hybridized complex. Dentine surface exhibited multiple amorphous clumps of material scattered and grouped as dense network of buttons-like materials, rounding (asterisk) or occluding (arrow) the entrance of tubules. Tubules appeared occluded (totally or partially) or empty. Dentine

(intertubular and peritubular) was strongly mineralised. Espectrum from energy dispersive analysis, attained at zone 34, is showing elemental composition of phosphorous (P), calcium (Ca), and zinc (Zn). Abbreviations: SEB: SE-Bond, SEB·P: SE-Bond primer, SEB·Bd: SE-Bond bonding. ZnO, zinc oxide; $ZnCl_2$, zinc chloride.

FIGURE 1

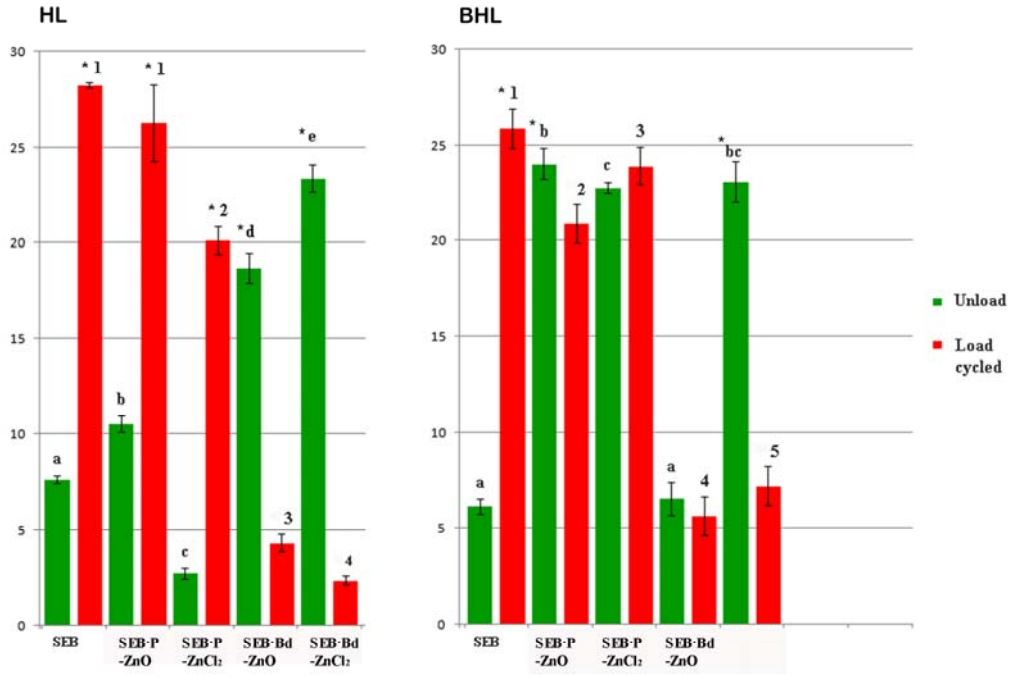

FIGURE 2

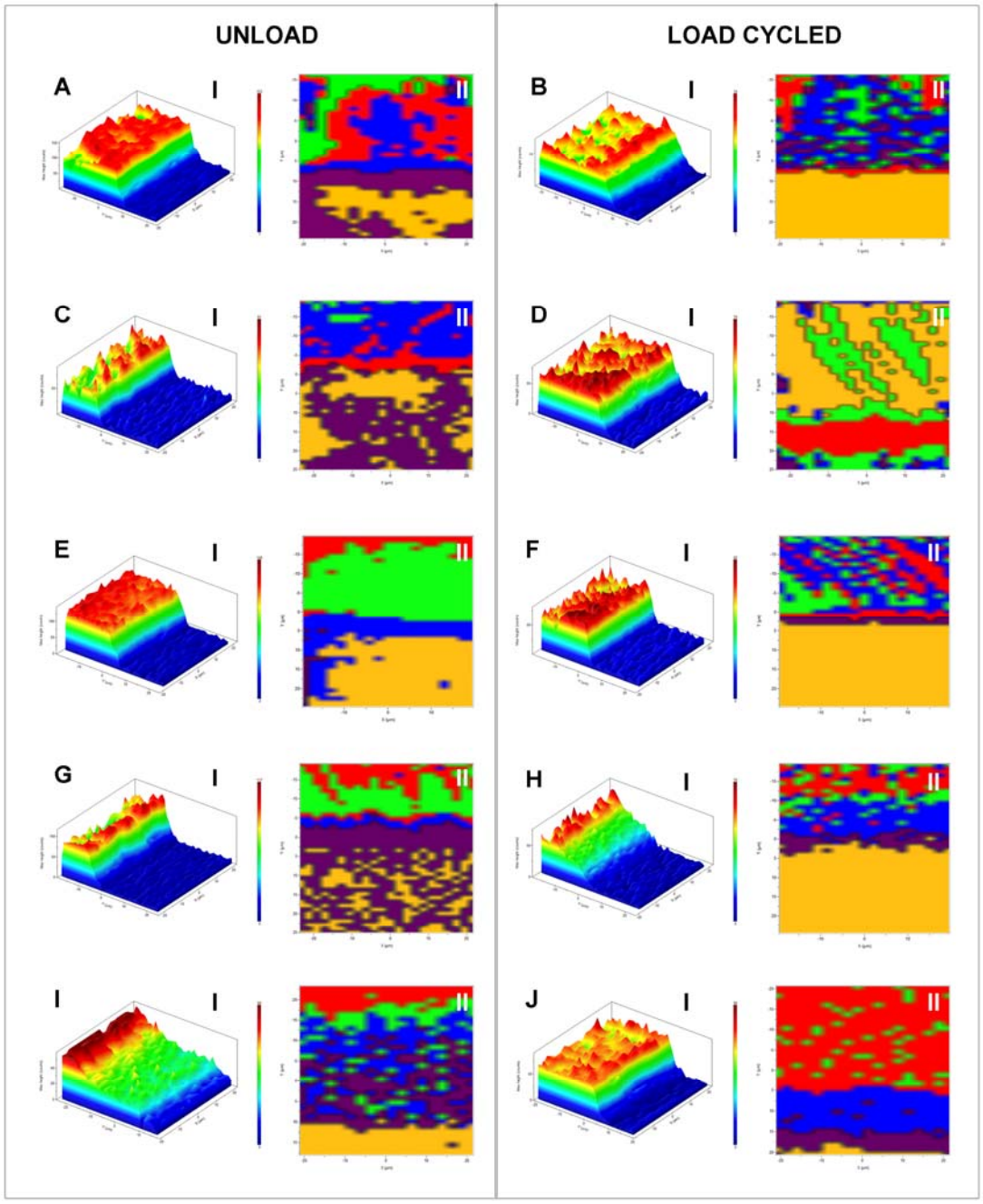
UNLOAD
LOAD CYCLED
A
I
II
B
I
II
C
I
II
D
I
II
E
I
II
F
I
II
G
I
II
H
I
II
I
I
II
J
I
II

FIGURE 3

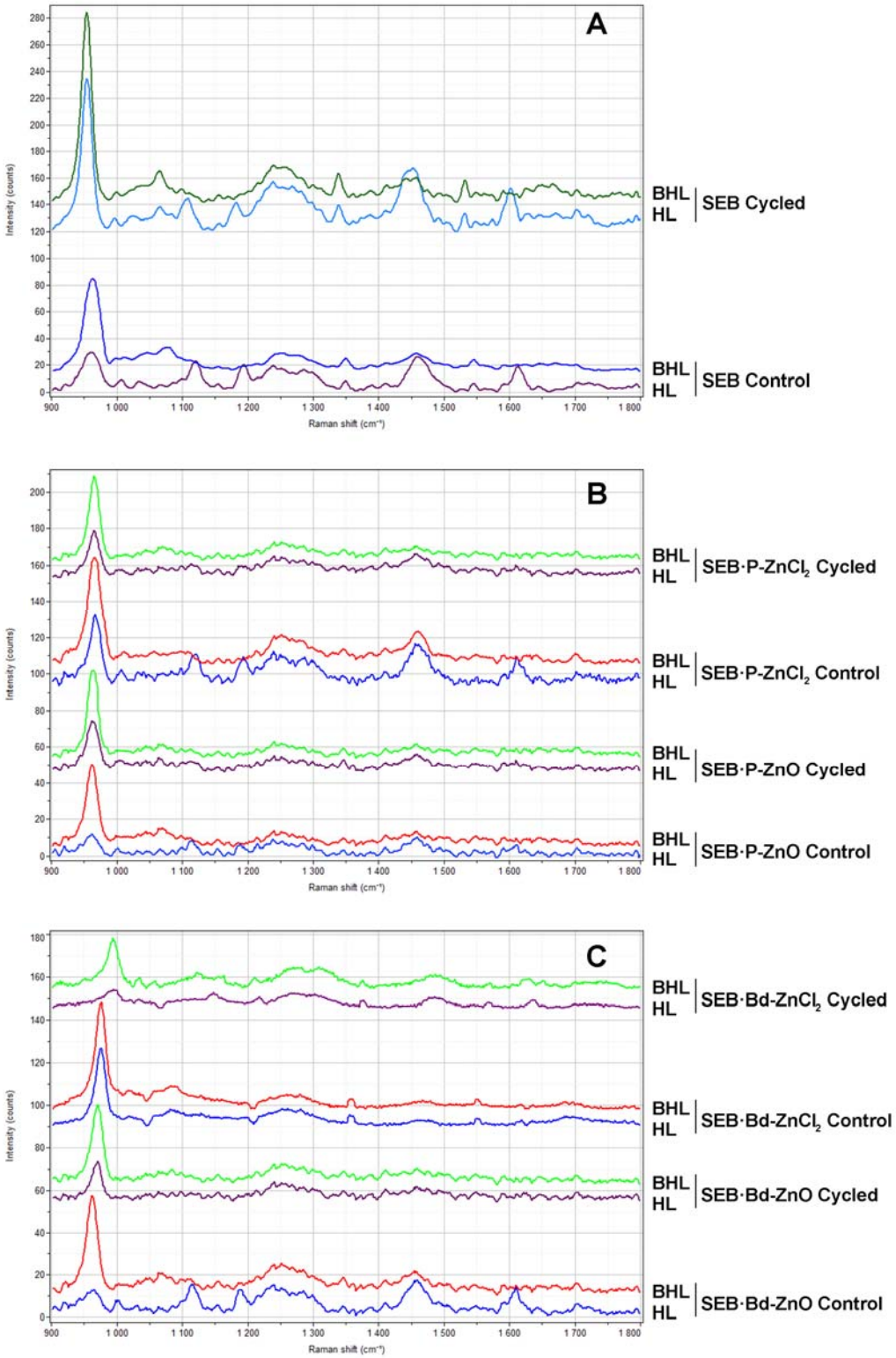
A
B
C
Intensity (counts)
Raman shift (cm⁻¹)
BHL
HL
SEB Cycled
SEB Control
SEB·P-ZnCl2 Cycled
SEB·P-ZnCl2 Control
SEB·P-ZnO Cycled
SEB·P-ZnO Control
SEB·Bd-ZnCl2 Cycled
SEB·Bd-ZnCl2 Control
SEB·Bd-ZnO Cycled
SEB·Bd-ZnO Control

FIGURE 4

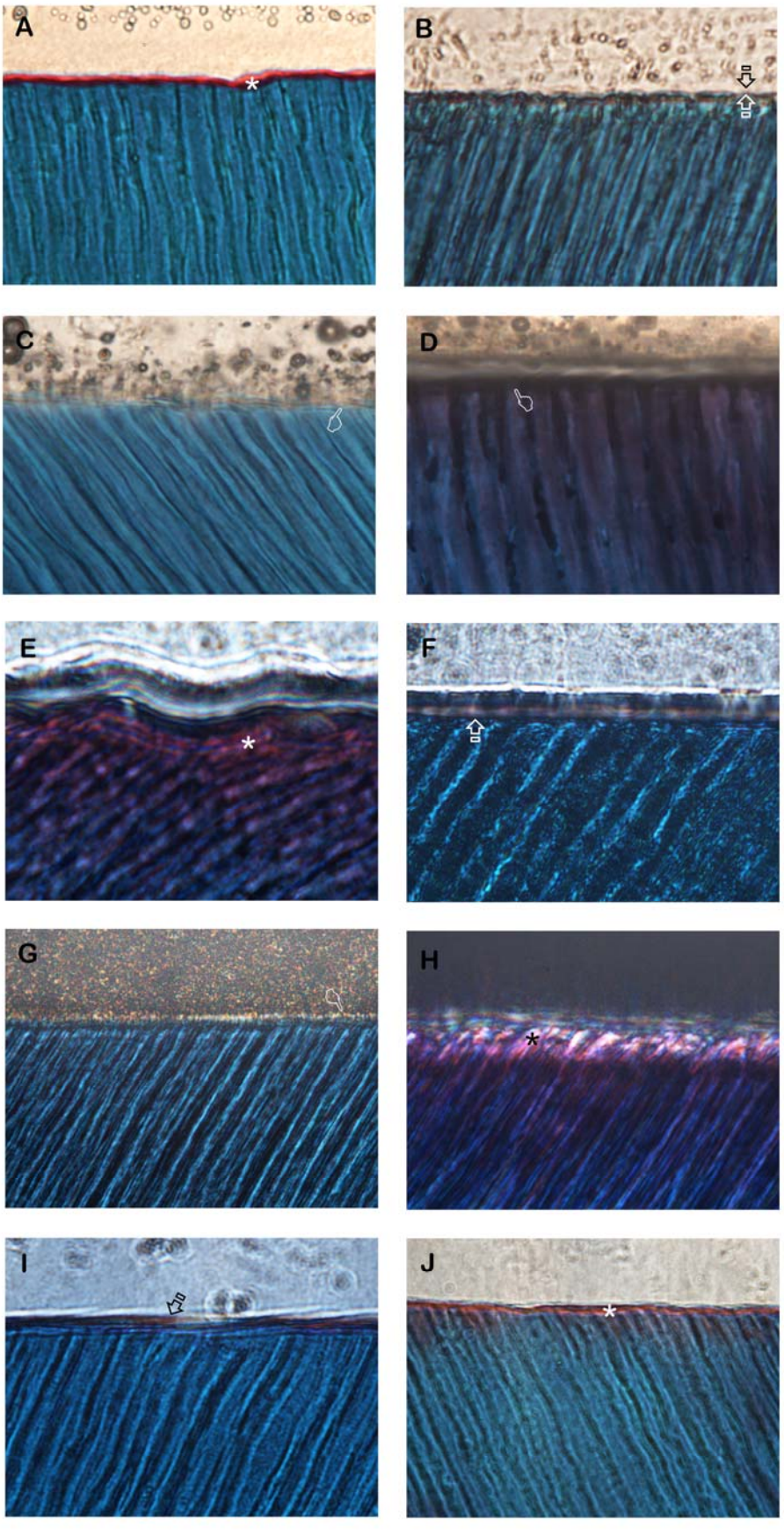

FIGURE 5

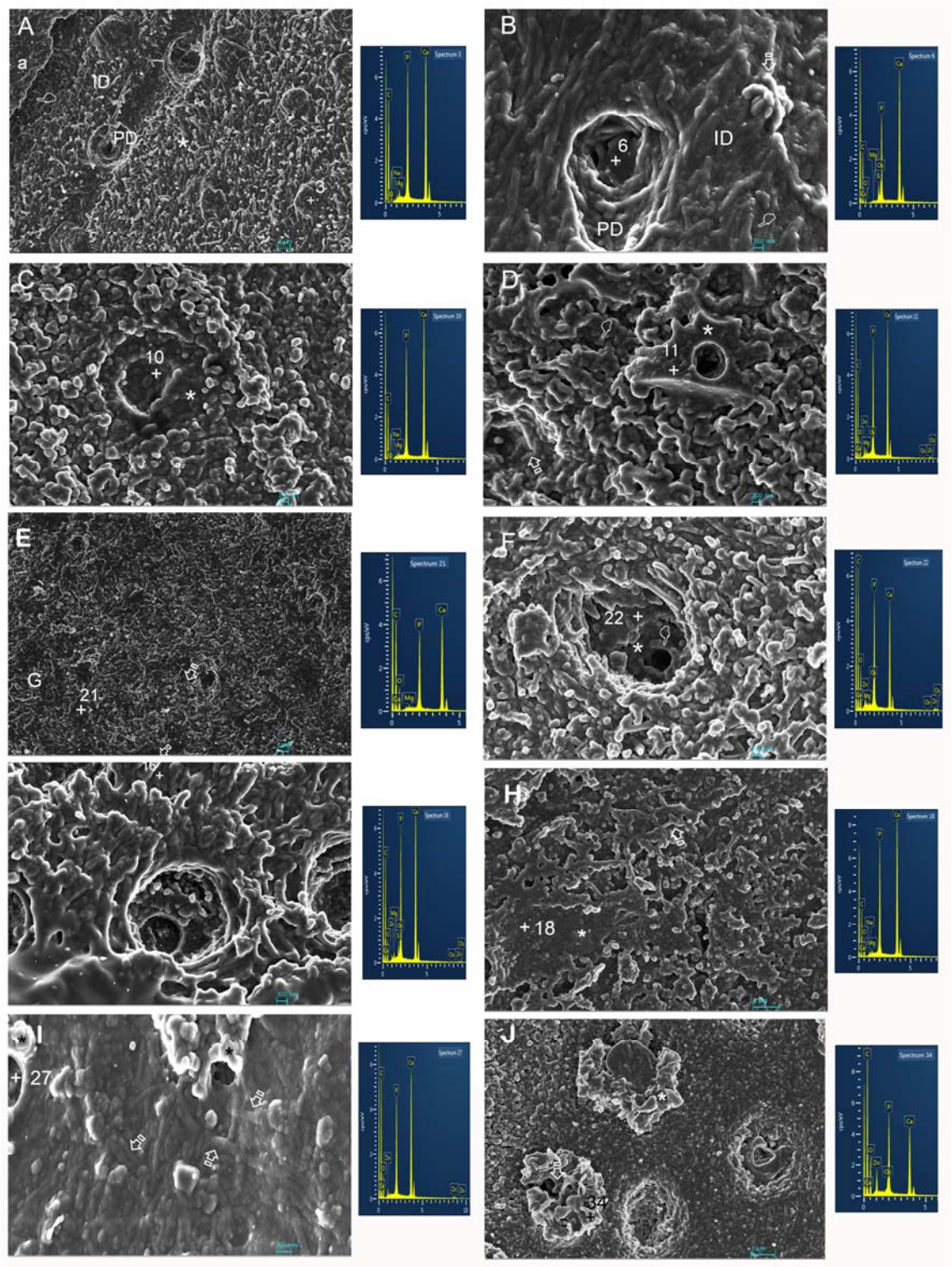

Table 1. Materials and chemicals used in this study and respective manufacturers, basic formulation and mode of application.

Product details	**Basic formulation**	**Mode of application**
Clearfil SE Primer and Bond (SEB) (Kuraray, Japan)	***Primer*** **(SEB·P)** MDP, HEMA, camphorquinone, N, N-Diethanol-p-toluidine, water ***Bond*** **(SEB·Bd)** Bis-GMA, MDP, HEMA, camphorquinone, N, N-Diethanol-p-toluidine, Silanated colloidal silica	**Adhesive application** Rinse with water Air-dry (5 s) Primer application (20 s) Air-dry (3 s) Adhesive application (10s) Light activation (15 s)
Zinc oxide (ZnO) (Panreac Química SA, Barcelona, Spain).		
Zinc chloride 2-hydrate powder ($ZnCl_2$) (Sigma Aldrich, St. Louis, MO, USA).		
X-FlowTM (Dentsply, Caulk, UK)	Strontium alumino sodium fluorophosphorsilicate glass, di- and multifunctional acrylate and methacrylate resins, DGDMA, highly dispersed silicon dioxide UV stabilizer, ethyl-4-dimethylaminobenzoate camphorquinone, BHT, iron pigments, titanium dioxide	
SBFS (pH=7.45)	NaCl 8.035 g $NaHCO_3$ 0.355 g KCl 0.225 g $K_2HPO_4 \cdot 3H_2O$ 0.231 g, $MgCl_2 \cdot 6H_2O$ 0.311 g 1.0 M – HCl 39 ml $CaCl_2$ 0.292 g Na_2SO_4 0.072 g Tris 6.118 g 1.0 M – HCl 0–5 ml	

Abbreviations: MDP:Methacryloyldodeylphosphate; HEMA: 2-hydroxyethyl methacrylate; Bis-GMA: bisphenol A diglycidyl methacrylate; DGDMA: diethyleneglycol dimethacrylate phosphate; BHT: butylated hydroxytoluene; SBFS: simulated body fluid solution; NaCl: sodium chloride; $NaHCO_3$: sodium bicarbonate; KCl: potassium chloride; $K_2HPO_4 \cdot 3H_2O$: potassium phosphate dibasic trihydrate; $MgCl_2 \cdot 6H_2O$: magnesium chloride hexahydrate; HCl: hydrogen chloride; $CaCl_2$: Calcium chloride; Na_2SO_4: sodium sulfate; Tris: tris(hydroxylmethyl) aminomethane; SBFS: simulated body fluid solution; NaCl: sodium chloride; $NaHCO_3$: sodium bicarbonate; KCl: potassium chloride; $K_2HPO_4 \cdot 3H_2O$: potassium phosphate dibasic trihydrate; $MgCl_2 \cdot 6H_2O$: magnesium chloride hexahydrate; HCl: hydrogen chloride; $CaCl_2$: Calcium chloride; Na_2SO_4: sodium sulfate; Tris: tris(hydroxylmethyl) aminomethane.

Table 2. Mean and standard deviation of microtensile bond strength values (MTBS), in MPa, and percentage distribution (%) of failure mode (A: Adhesive; M: Mixed), obtained for the different experimental groups.

	UNLOADED			**LOAD CYCLED**		
	A %	**M %**	**Mean (SD) MPa**	**A %**	**M %**	**Mean (SD) MPa**
SEB	39	61	38.48 (5.22) A	71	29	33.96 (3.69) A
SEB·P-ZnO	36	64	33.06 (5.25) AB	78	22	33.77 (3.97) A
SEB·P-$ZnCl_2$	55	45	26.15 (4.34) B	67	33	25.84 (2.94) B
SEB·Bd-ZnO	40	60	34.05 (3.24) AB	80	20	33.56 (3.58) A
SEB·Bd-$ZnCl_2$	49	51	30.05 (4.44) AB	72	28	28.27 (3.40) AB

Identical letters indicate no significant difference in columns after Student-Newman-Keuls or Student's t tests ($p < 0.05$). No differences were found between load and unloaded groups.
Abbreviations: SEB: SE-Bond; SEB·P: SE-Bond primer; SEB·Bd: SE-Bond bonding; ZnO: zinc oxide; $ZnCl_2$: zinc chloride.

Table 3a. Mineral related peaks and ratios in SEB-treated sound dentine surfaces.

			Relative Presence of Mineral				FWHM	GMC Ratio C/P	PPR Ratio phosphate peak /healthy substratum
			Phosphate [961]			Carbonate [1070]			
			Peak	Area	RMC	Peak	Phosphate		
SEB	Control	HL	25.62	600.13	4.72	4.53	19.30	0.18	0.29
		BHL	45.86	1127.7	12.70	8.64	19.31	0.19	0.52
	Load cycled	HL	110.01	2640.62	17.92	15.05	19.33	0.14	1.26
		BHL	142.39	3485.3	23.69	22.61	19.33	0.16	1.63
SEB·P-ZnO	Control	HL	11.98	388.97	2.78	3.87	25.73	0.32	0.14
		BHL	46.58	1146.27	13.39	8.36	19.30	0.18	0.53
	Load cycled	HL	24.36	599.69	8.49	5.37	19.30	0.22	0.28
		BHL	50.17	1235.17	13.17	8.63	19.29	0.17	0.57
SEB·P-$ZnCl_2$	Control	HL	32.47	800.88	5.56	4.41	19.27	0.14	0.37
		BHL	60.75	1499.53	10.77	5.64	19.31	0.09	0.70
	Load cycled	HL	22.44	641.32	6.41	4.59	22.50	0.20	0.26
		BHL	47.85	1178.79	18.06	7.08	19.29	0.15	0.55
SEB·Bd-ZnO	Control	HL	11.09	360.7	2.54	4.08	25.79	0.37	0.13
		BHL	48.15	1184.95	12.35	8.61	19.30	0.18	0.55
	Load cycled	HL	17.86	511.24	8.97	4.02	22.48	0.23	0.20
		BHL	40.99	1012.55	16.01	5.04	19.31	0.12	0.47
SEB·Bd-$ZnCl_2$	Control	HL	40.41	988.31	6.84	9.36	19.25	0.23	0.46
		BHL	47.05	1348.47	6.39	9.82	22.46	0.21	0.54
	Load cycled	HL	6.82	223.33	1.83	3.09	25.57	0.45	0.08
		BHL	22.99	568.61	9.38	5.9	19.19	0.26	0.26

Abbreviations: RMC: Relative Mineral Concentration between mineral/Phenyl (1003); FWHM: Full-width half-maximum; GMC: Gradient in Mineral Content; PPR: Phosphate Peaks Ratio. Peaks positions are expressed in cm^{-1}.

Table 3b. Organics related peaks and ratios in SEB-treated sound dentine surfaces.

			Normalization	Crosslinking				Nature of collagen								
			Phenyl [1003]	Pyrid. [1032]	Ratio 1031/1001	Ratio phenyl/CH_2 [1003/CH]	AGEs-Pentosidine [1550]	A-III [1246-1270]	CH_2 [1450]	A-I [1655-1667]	Ratio Amide I/ Amide III	Ratio Amide III/ CH_2	Ratio Amide I/ CH_2	Ratio Amide III/ AGEs-Pentosidine	Ratio Amide I/ AGEs-Pentosidine	α-helices [1340]
SEB	Control	HL	5.43	3.72	0.69	0.36	3.15	9.17	15.06	1.68	0.18	0.61	0.11	2.91	0.53	4.18
		BHL	3.61	4.16	1.15	0.64	3.5	7.43	5.68	2.89	0.39	1.31	0.51	2.12	0.83	6.06
	Load cycled	HL	6.14	7.63	1.24	0.14	4.4	30.33	43.91	9.70	0.32	0.69	0.22	6.89	2.20	16.32
		BHL	6.01	10.78	1.79	0.34	5.42	25.17	17.65	12.29	0.49	1.43	0.70	4.64	2.27	20.39
SEB·P-ZnO	Control	HL	4.31	3.32	0.77	0.41	3.68	6.46	10.53	1.93	0.30	0.61	0.18	1.76	0.52	3.63
		BHL	3.48	4.79	1.38	0.54	3.65	8.79	6.42	3.48	0.40	1.37	0.54	2.41	0.95	4.94
	Load cycled	HL	2.87	3.65	1.27	0.49	4.05	7.27	5.83	3.24	0.45	1.25	0.56	1.80	0.80	6.30
		BHL	3.81	4.83	1.27	0.60	3.69	8.73	6.40	3.68	0.42	1.36	0.58	2.37	1.00	6.18
SEB·P-$ZnCl_2$	Control	HL	5.84	4.61	0.79	0.29	3.1	14.83	19.82	2.07	0.14	0.75	0.10	4.78	0.67	4.40
		BHL	5.64	5.00	0.89	0.31	2.63	14.61	18.14	3.27	0.22	0.81	0.18	5.56	1.24	5.59
	Load cycled	HL	3.50	3.86	1.10	0.33	2.83	9.51	10.56	1.65	0.17	0.90	0.16	3.36	0.58	3.81
		BHL	2.65	3.88	1.46	0.43	3.21	8.73	6.12	3.35	0.38	1.43	0.55	2.72	1.04	4.52
SEB·Bd-ZnO	Control	HL	4.36	2.78	0.64	0.47	3.88	10.75	9.25	2.11	0.20	1.16	0.23	2.77	0.54	5.01
		BHL	3.90	4.38	1.12	0.49	3.6	11.86	8.02	3.61	0.30	1.48	0.45	3.29	1.00	6.37
	Load cycled	HL	1.99	2.12	1.07	0.31	3.65	8.04	6.46	2.08	0.26	1.24	0.32	2.20	0.57	4.30
		BHL	2.56	3.07	1.20	0.43	3.6	8.64	5.99	2.79	0.32	1.44	0.47	2.40	0.78	4.86
SEB·Bd-$ZnCl_2$	Control	HL	5.91	4.16	0.70	1.22	5.26	9.98	4.84	3.80	0.38	2.06	0.79	1.90	0.72	7.05
		BHL	7.36	3.05	0.41	1.23	6.25	9.57	5.96	5.22	0.55	1.61	0.88	1.53	0.84	7.93
	Load cycled	HL	3.73	3.94	1.06	0.60	3.46	6.50	6.17	2.01	0.31	1.05	0.33	1.88	0.58	3.68
		BHL	2.45	2.46	1.00	0.64	3.28	7.07	3.84	2.11	0.30	1.84	0.55	2.16	0.64	4.69

Abbreviations: A: Amide; Pyrid: Pyridinium; AGEs: Advanced glycation end products. Peaks positions are expressed in cm^{-1}.

Table 3c. Adhesive related peaks and ratios in SEB-treated sound dentine surfaces.

			Degree of Adhesive Presence				
			DC [1637/1608]	Bis-GMA Penetration [1113/A-I]	Adhesive Penetration [1453/1667]	Carbonyl Group [1720]	CH_2 def [1453]
SEB	Control	HL	0.29	7.27	8.96	2.76	15.06
		BHL	1.74	1.35	1.97	1.59	5.68
	Load cycled	HL	1.06	2.17	4.53	8.8	43.91
		BHL	2.43	0.43	1.44	4.41	17.65
SEB·P-ZnO	Control	HL	0.49	4.25	5.46	2.5	10.53
		BHL	2.04	1.11	1.84	1.68	6.42
	Load cycled	HL	1.65	6.31	1.80	1.82	5.83
		BHL	2.19	1.06	1.74	1.97	6.4
SEB·P-$ZnCl_2$	Control	HL	0.27	6.28	9.57	3.64	19.82
		BHL	0.43	2.29	5.55	2.37	18.14
	Load cycled	HL	0.56	6.31	6.40	2.29	10.56
		BHL	1.78	1.20	1.83	1.77	6.12
SEB·Bd-ZnO	Control	HL	0.55	3.64	4.38	2.32	9.25
		BHL	1.56	1.45	2.22	1.82	8.02
	Load cycled	HL	1.00	1.72	3.11	2.03	6.46
		BHL	1.88	1.34	2.15	2.06	5.99
SEB·Bd-$ZnCl_2$	Control	HL	0.89	1.42	1.27	1.81	4.84
		BHL	0.92	1.24	1.14	2.95	5.96
	Load cycled	HL	1.05	1.84	3.07	2.13	6.17
		BHL	0.87	1.32	1.82	1.84	3.84

Abbreviations: DC: Degree of conversion of adhesive; Bis-GMA: bisphenol A diglycidyl methacrylate.
Peaks positions are expressed in cm^{-1}.